Digest Journal of Nanomaterials and Biostructures

Dig. J. Nanomater. Bios. **2026**; 21(2): 55238
https://doi.org/10.31083/DJNB55238

Original Research

Biochar-Enhanced Textile-Based Piezoresistive Sensors for Real-Time Flow and Pressure Monitoring in Fluidic Systems

Blessing Sam Raj R[1,*], Vimal Samsingh R[1]

[1]Department of Mechanical Engineering, Sri Sivasubramaniya Nadar College of Engineering, 603110 Tamil Nadu, India
*Correspondence: blessingsamrajr@gmail.com (Blessing Sam Raj R)

Academic Editor: Carmen-Georgeta Ristoscu
Submitted: 13 January 2026 Revised: 7 March 2026 Accepted: 19 March 2026 Published: 24 June 2026

Abstract

Progress in flexible piezoresistive sensors is essential for applications in wearable technologies and real-time fluid monitoring systems. This study presents the fabrication and performance of textile-based sensors coated with *Senna siamea* biomass–derived biochar at different loadings via a dip-coating technique. Biochar structural and surface characteristics were investigated using X-ray diffraction, Fourier transform infrared spectroscopy, and scanning electron microscopy. Sensors with biochar loadings of 1, 5, 10, and 15 wt % were integrated into a custom-designed flow setup to examine the evolution of their electrical resistance under varying water flow rates and applied pressures. Sensors with low biochar loadings, particularly 5 wt %, demonstrated superior sensitivity, stability, and linearity, showing distinct resistance variations corresponding to pressure changes induced by water flow. Higher biochar contents resulted in agglomeration and reduced conductivity, thereby diminishing sensor performance. The sensors exhibited reliable output under both static and dynamic conditions, thus holding promise for wearable health monitoring and industrial fluid control. This work shows the potential of biochar as a sustainable and cost-effective material for next-generation piezoresistive sensing platforms.

Keywords: biochar; piezoresistive sensor; textile-based sensor; flow and pressure monitoring

1. Introduction

The evolution of flexible piezoresistive pressure sensors has significantly advanced the development of wearable electronics, electronic skin (e-skin), and intelligent human–machine interfaces. These sensors, which are capable of converting mechanical stimuli into electrical signals, have applications in health monitoring, robotics, and artificial intelligence systems [1,2]. Recent studies have demonstrated the integration of piezoresistive sensors into wearable devices for real-time physiological monitoring, such as pulse detection and motion tracking [3,4]. The adaptability and sensitivity of these sensors make them ideal for applications that require conformability and responsiveness to dynamic mechanical forces [5,6].

Despite their advantages, the flammability of conventional sensor materials poses significant safety concerns, especially in applications involving electrical circuits and human contact. To address this issue, researchers have explored conductive textile fabrics for sensor development [7]. The incorporation of materials, such as polydimethylsiloxane (PDMS), carbonized aerogels, and conductive polymers, has led to the creation of sensors that maintain performance while enhancing safety [8,9]. These advancements are crucial for developing reliable and safe wearable sensors suitable for various environments, particularly in biomedical and hazardous field conditions [10].

Derived from biomass pyrolysis, biochar is a carbon-rich material that has emerged as a promising candidate for advancing the performance of piezoresistive sensors. Its porous structure and electrical conductivity contribute to improved sensitivity and stability in pressure sensing applications [11,12]. Studies have shown that biochar-based composites can be effectively utilized in flexible piezoresistive sensor fabrication, offering sustainable and cost-effective alternatives [13,14]. Biochar's network-like microstructure facilitates tunneling conduction mechanisms, enabling it to perform comparably to or better than traditional materials, such as carbon black and graphene, in pressure sensor applications [15,16].

Although highly conductive nanomaterials, such as carbon nanotubes (CNTs) and graphene, have been widely investigated for flexible piezoresistive sensing applications owing to their superior electrical conductivity, their large-scale implementation is often limited by high material cost, dispersion challenges, and complex fabrication processes [15,17]. In contrast, biochar derived from biomass represents a sustainable and cost-effective carbon source with inherent hierarchical porosity and tunable graphitic domains formed during pyrolysis [14]. The disordered aromatic carbon framework in biochar facilitates pressure-dependent percolation and electron tunneling conduction mechanisms, which are highly desirable for piezoresistive sensing performance [15,16]. Furthermore, the presence of oxygen-containing functional groups on biochar surfaces enhances interfacial adhesion with textile substrates, improving coating stability and mechanical robustness [11,18]. Owing to these structural, electrical, and environmental advantages, biochar provides a balanced combination of conductivity,

sustainability, and process simplicity, making it a promising alternative to conventional conductive nanomaterials for textile-based sensing platforms.

Recent studies have demonstrated the effectiveness of biomass-derived carbon materials in flexible piezoresistive sensing applications. For example, carbonized cellulose aerogels and porous biomass-derived carbon frameworks have been reported to exhibit high compressibility and tunable electrical responses owing to their hierarchical pore structures [11,14]. Textile-based carbonized fabrics have also demonstrated enhanced strain-induced resistance variation arising from percolation-based conduction within disordered carbon networks [16]. Furthermore, reviews on flexible piezoresistive sensors highlight that electron tunneling and contact resistance modulation within porous carbon systems play a dominant role in determining sensitivity and linearity [15]. Biowaste-derived multifunctional sensors have demonstrated environmental stability and sustainability advantages compared to synthetic nanocarbon materials [18]. However, most reported studies have primarily focused on compression-based sensing under direct mechanical loading, and limited investigations have explored simple dip-coated biochar textiles for flow-induced pressure monitoring in enclosed fluidic systems. This gap motivates the present study.

In this study, we developed a coated textile fabric for use in piezoresistive pressure sensors through a dip-coating process involving biochar. The sensors were fabricated with varying biochar concentrations of 1, 5, 10, and 15 wt %, and integrated into a system designed to measure the flow rate and monitor pressure in a circular pipe. The sensors operate by detecting changes in the electrical resistance caused by fluid flow, thereby providing real-time data on pressure variations [17,19,20]. Our findings indicate that the sensor with 5 wt % biochar exhibited the highest sensitivity, highlighting the potential of biochar-based sensors in fluid monitoring applications. This work contributes to the development of sustainable and textile-based flow-sensing platforms and supports the advancement of next-generation sensing systems for industrial applications [21,22,23,24,25].

2. Materials and Methods

2.1 Biomass

Senna siamea biomass was collected from local farms in Thiruporur, Tamil Nadu. The collected biomass was air-dried at room temperature for seven days. To eliminate adhering impurities and foreign materials, the biomass was first rinsed thoroughly with tap water five times, followed by a final wash using deionized water. The cleaned biomass was then oven-dried at 80 °C for 24 h. Subsequently, the dried material was partially pulverized into smaller particles using a mechanical pulverizer. A schematic representation of the entire preparation process is presented in Fig. 1.

2.2 Carbonization of Biomass

Biochar was prepared by carbonization of *Senna siamea* biomass using a biomass conversion unit based on the American Society for Testing Materials E1755-01 test method, and chemical analysis of biomass. The biomass was carbonized at 550 °C at a controlled heating rate of 10 °C min^{-1}. Air-dried powdered biomass was placed in a conversion chamber that could maintain a slow pyrolysis aspect with a nitrogen atmosphere. Simultaneously, slow cooling was maintained in the furnace after carbonization. In Fig. 2, the carbonization process of biochar is graphically illustrated.

2.3 Characterization of Biochar

X-ray diffraction (XRD) analysis was performed using a high-resolution PANalytical X-ray diffractometer (PANalytical, Almelo, Netherlands) equipped with a radiation source at 1.8 kW, and the measurements were conducted at room temperature. The diffraction data were recorded over a 2θ range of 10–90° at a scanning rate of 1° min^{-1}. Fourier transform infrared (FTIR) spectroscopy was conducted using a Bruker Alpha-T spectrometer (Bruker, Karlsruhe, Germany) in the spectral range of 4000–500 cm^{-1}. The surface morphology of the coated samples was examined using a field-emission scanning electron microscope (FESEM) (Thermo Fisher Scientific, Apreo 2S, Waltham, MA, USA).

2.4 Sample Preparation

In this study, biochar obtained from *Senna siamea* biomass was used for sample preparation. Dip coating is one of the universal methods followed for coating. A polyester textile fabric with a size of 100 mm × 25 mm was used for dip coating. The coating solution was prepared with 100 mL of deionized water and biochar at various percentages, and the solution was magnetically stirred for 3 h.

2.5 Experimental Setup

The experimental setup designed exclusively for measuring resistance changes using the fabricated biochar sensor is depicted in Fig. 3A. This setup comprised a series of pipes, within which the sensor was installed in a detachable section, as illustrated in the enlarged image in Fig. 3A. The detachable section featured a cutaway where the sensor was positioned and sealed with a waterproof two-part adhesive resin and hardener combination, which, upon drying, became leak-proof.

The sensor terminal leads were interfaced with a data acquisition system that continuously recorded the monitoring signals as variations in electrical resistance. Water circulation within the experimental setup was facilitated by a pump that transferred fluid from the reservoir through a network of pipes. The flow pressure was displayed using a pressure gauge and could be regulated via an adjacent control valve. To improve measurement reliability,

Fig. 1. Schematic representation of the biochar production process.

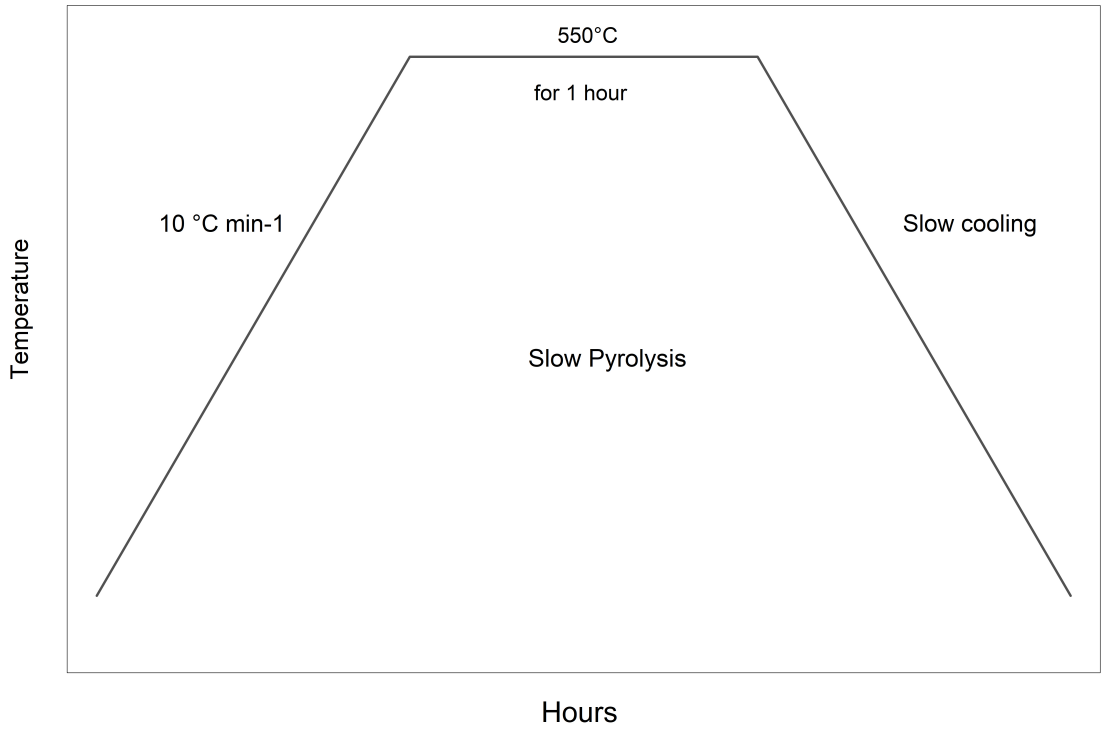

Fig. 2. Carbonization of biomass.

a digital pressure gauge was additionally used for precise pressure monitoring. The outlet of the pipeline was routed back to the fluid tank to maintain consistent water circulation throughout the system. A schematic representation of the experimental setup and its components is illustrated in Fig. 3B. The pipeline used in the experiment had a nominal diameter of 25 mm and an outer diameter of 33.4 mm. The detachable pipe section was 250 mm long and was fitted with 25 mm polyvinyl chloride union couplings at both ends to facilitate easy assembly and disassembly [26].

3. Results

3.1 XRD for BC

The XRD pattern of biochar produced at 550 °C, shown in Fig. 4, exhibits a broad diffraction peak in the 2θ range of 22–24°, corresponding to the (002) plane of the carbon structures. The broad peak indicates the presence of a predominantly disordered carbon structure formed during biomass pyrolysis [11,14]. No sharp crystalline peaks were observed in the diffraction pattern, suggesting the absence of highly ordered graphite phases. These results indicate that the synthesized biochar mainly consisted of amorphous and turbostratic carbon domains.

3.2 Fourier Transform Infrared (FTIR)

The FTIR spectrum of the synthesized biochar is shown in Fig. 5. A broad absorption band appears at approximately 3350 cm^{-1}, which is associated with O–H stretching vibrations originating from hydroxyl groups present in biomass-derived carbon materials [11,14]. A peak observed near 1625–1630 cm^{-1} corresponds to C=O stretching or aromatic C=C vibrations, indicating the presence of conjugated carbon structures formed during pyrol-

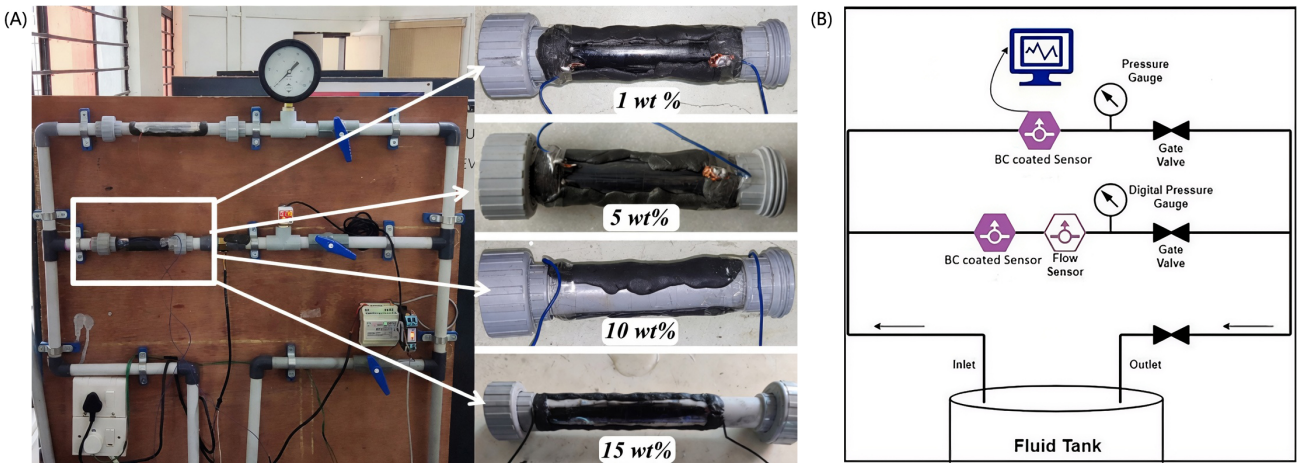

Fig. 3. Experimental setup and schematic representation of the biochar-coated textile sensor system for flow-induced pressure measurements. (A) Experimental setup with the attachments. (B) Schematic representation of the experimental setup used for pressure-sensing measurements. BC, biochar.

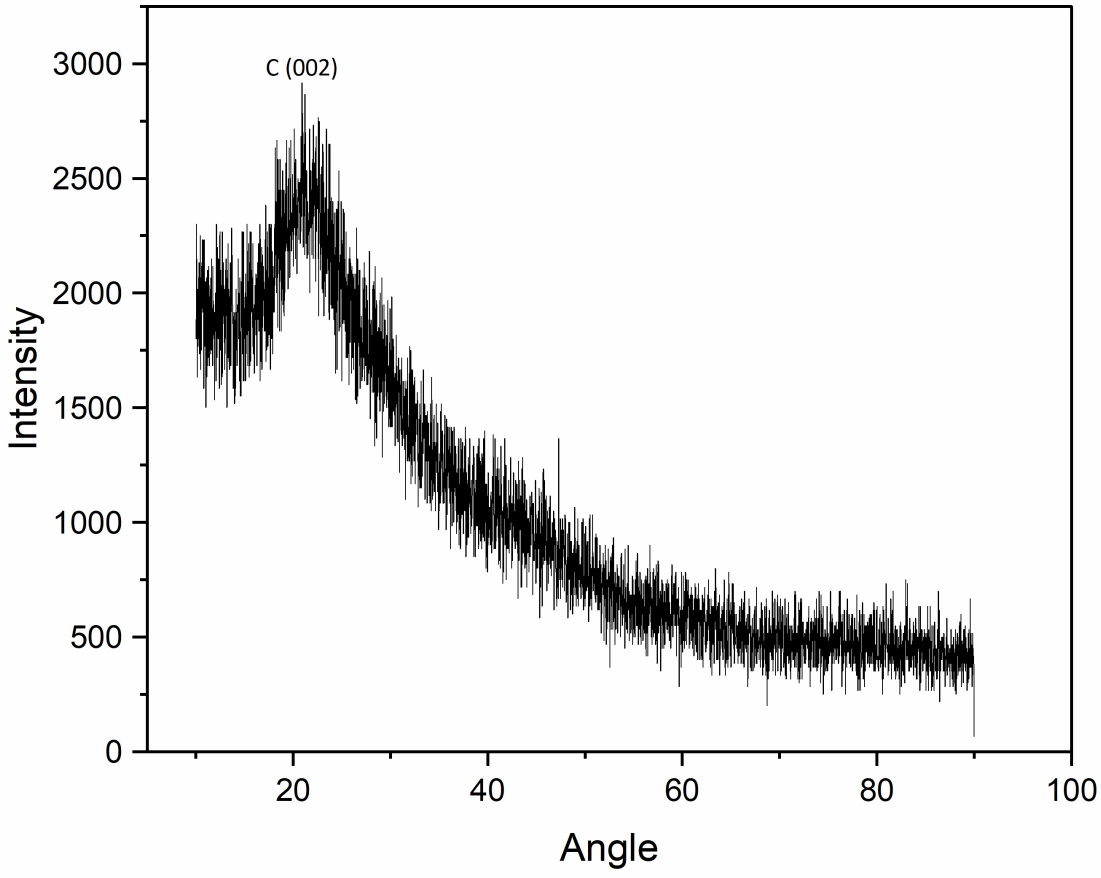

Fig. 4. XRD characterization of biochar. XRD, X-ray diffraction.

ysis [11,15,18]. In addition, a band at approximately 1175–1180 cm^{-1} is attributed to C–O stretching vibrations from alcohols, ethers, or phenolic functional groups typically found in biochar materials [14,18]. These peaks indicate the presence of oxygen-containing functional groups in the synthesized biochar.

3.3 XRD for Coated Samples

XRD analysis was performed to examine the structural characteristics of biochar-coated textile samples with different biochar loadings of 1 wt %, 5 wt %, 10 wt %, and 15 wt %. The XRD patterns are presented in Fig. 6. All samples exhibited a broad diffraction peak centered around 22°,

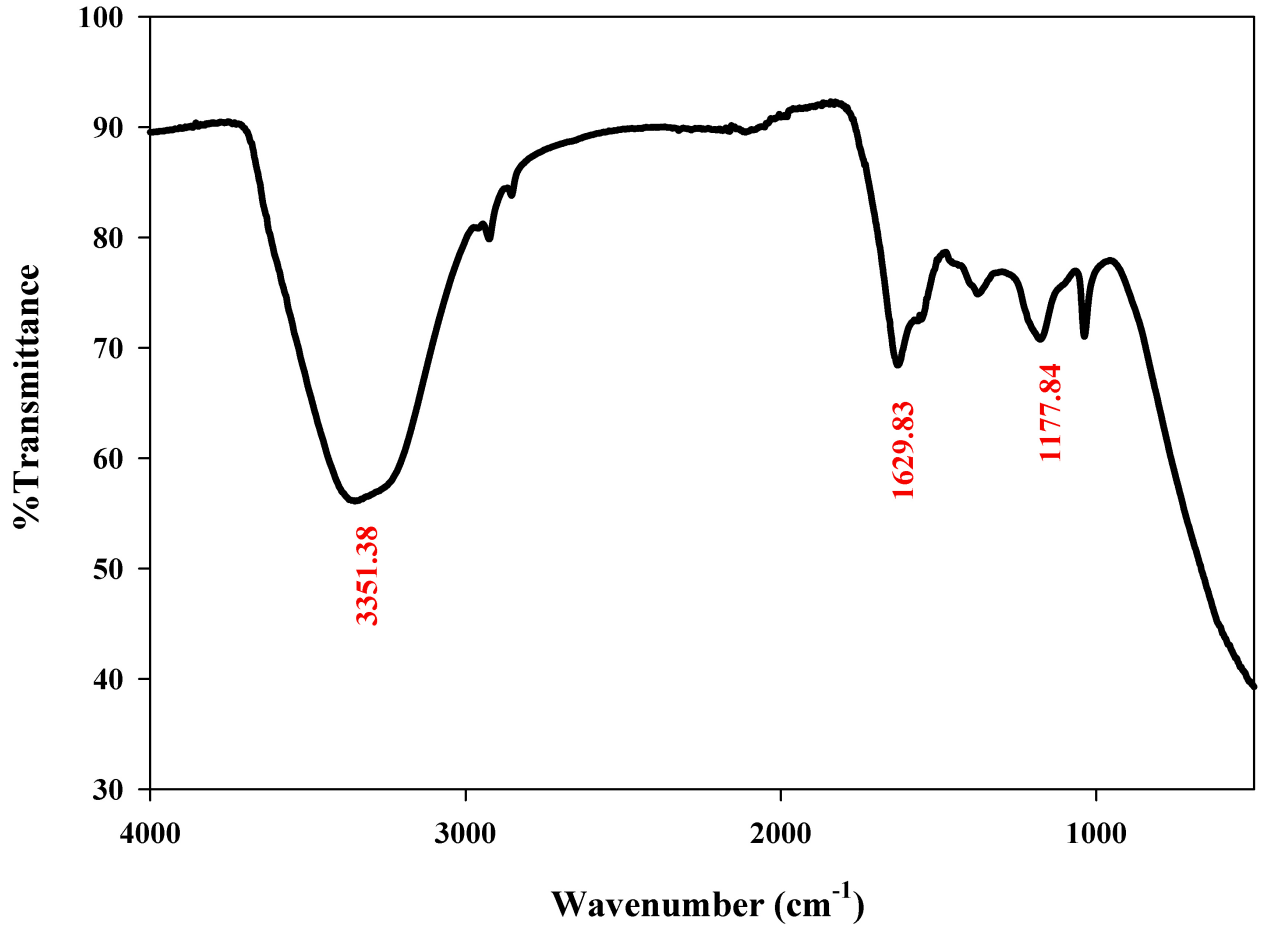

Fig. 5. Fourier transform infrared (FTIR) spectroscopy characterization of biochar.

corresponding to the (002) reflection of turbostratic carbon. As the biochar concentration increased from 1 wt % to 15 wt %, the intensity of this peak gradually increased. The broad diffraction peak indicated that the deposited biochar maintained a predominantly amorphous or turbostratic carbon structure across all concentrations.

3.4 Morphology Study

The surface morphology of biochar-coated textile samples with different biochar concentrations was examined using scanning electron microscopy (SEM), as shown in Fig. 7A–F. Fig. 7A shows the morphology of pristine biochar, which exhibits distinct particle boundaries and a porous texture characteristic of biomass-derived carbon materials. Fig. 7B shows aggregated biochar particles forming an interconnected porous structure with rough surfaces. The textile sample coated with 1 wt % biochar, shown in Fig. 7C, displays a thin and sparsely distributed layer of biochar particles along the fiber surfaces, where the underlying textile fibers remain clearly visible. The micrographs of the intermediate concentrations, shown in Fig. 7D and Fig. 7E for 5 wt % and 10 wt % biochar, respectively, illustrate a gradual increase in surface coverage. At 5 wt %, the biochar particles appear more uniformly distributed along the textile fibers, forming a more continuous coating layer. At 10 wt %, the coating becomes denser, and localized clusters of particles begin to appear. In contrast, Fig. 7F corresponding to the 15 wt % sample shows a heavily coated fiber surface with thick and irregular biochar layers. Large particle aggregates are observed, indicating reduced dispersion uniformity at higher biochar concentrations.

3.5 Flexibility Evaluation Under Bending

The mechanical flexibility of the optimized 5 wt % biochar-coated textile sensor was evaluated by measuring the resistance variation under different bending angles ranging from 0° to 180°. The electrical resistance of the sensor was recorded at each bending angle, and the relative resistance (R/R_0) was calculated with respect to the flat condition, where R_0 represents the initial resistance measured at 0° bending. As the bending angle increased, the relative resistance (R/R_0) gradually increased, indicating a measurable change in the electrical response of the sensor under mechanical deformation. As shown in Fig. 8, the relative resistance increased progressively with the bending angle, demonstrating that the textile-based sensor maintained electrical responsiveness under different bending conditions.

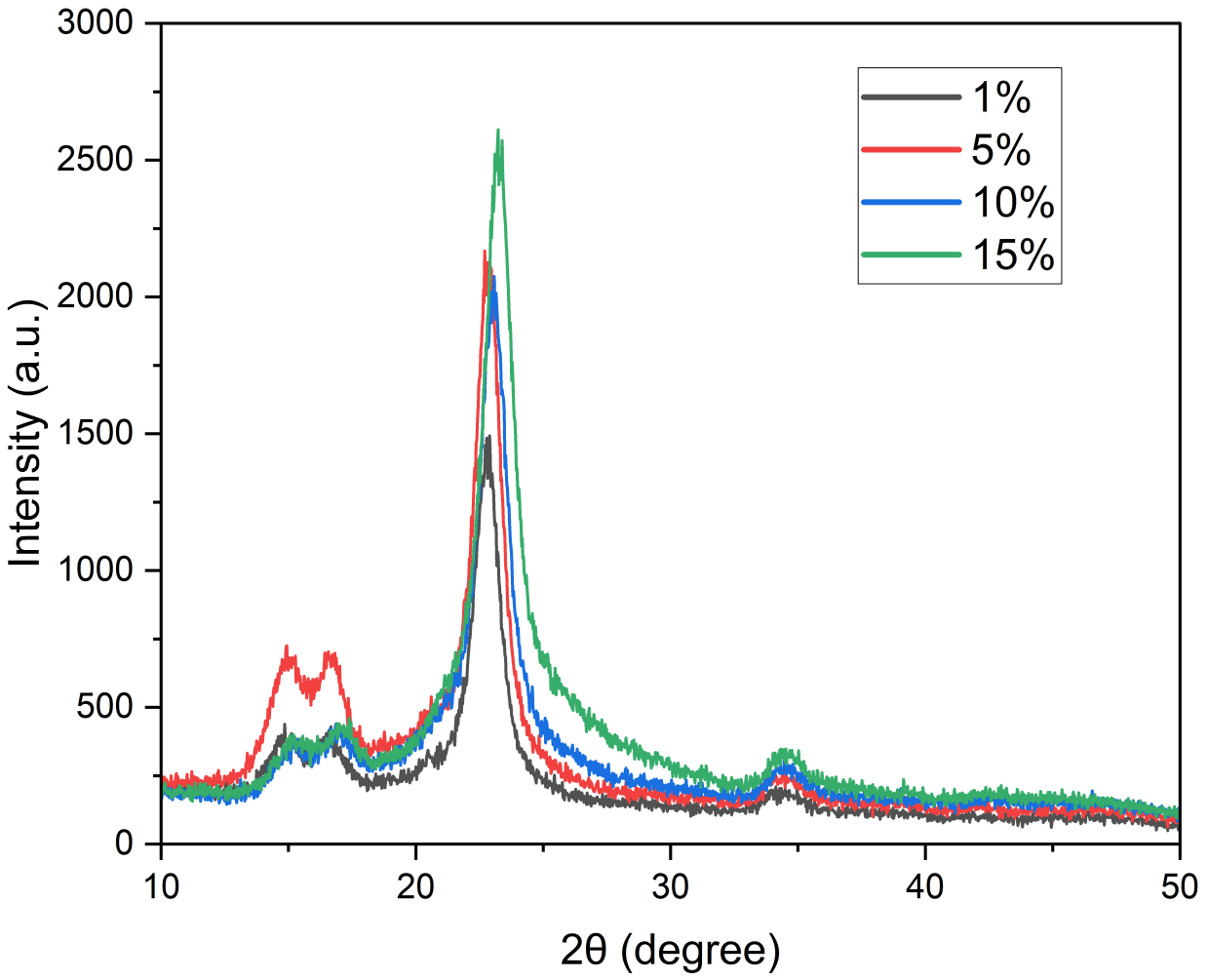

Fig. 6. XRD characterization of coated biochar samples.

3.6 Experimental Analysis—Stable Condition

To evaluate the stability of the biochar-coated textile sensors, the electrical resistance of the samples was monitored for 300 s under static, no-flow conditions. The measured resistance values for sensors containing 1 wt %, 5 wt %, 10 wt %, and 15 wt % biochar are shown in Fig. 9. The resistance values remained relatively stable throughout the measurement period, with only minor fluctuations. The 1 wt % sensor exhibited the lowest resistance of approximately 300 kΩ, whereas the 15 wt % sensor showed higher resistance values approaching 1100 kΩ. The sensors with 5 wt % and 10 wt % biochar exhibited intermediate resistance values with stable output during the testing period. These observations indicate the consistent electrical behavior of the sensors under static conditions.

Fig. 10 shows the variations in water flow rate (L/min) and pressure (bar) as functions of pump speed (rpm) in the experimental system. As the pump speed increased from 250 rpm to 2500 rpm, both the water flow rate and pressure showed a gradual increase. The water flow rate increased from approximately 5 L/min to 26 L/min, whereas the corresponding pressure increased from approximately 0.03 bar to 0.52 bar. The observed trend indicates a consistent relationship among pump speed, flow rate, and pressure in the experimental setup.

3.7 Experimental Analysis—Variable Condition

Fig. 11 illustrates the relationship between the relative resistance (R/R_0) of biochar-coated textile sensors and the water flow rate for different biochar loadings of 1 wt %, 5 wt %, 10 wt %, and 15 wt %. As the water flow rate increased from approximately 4 L/min to 25 L/min, the relative resistance values for all sensor compositions gradually increased. The 1 wt % sensor exhibited higher R/R_0 values in the range of approximately 2.6–2.65, whereas the 5 wt % sensor showed values around 2.4–2.45. The sensors containing 10 wt % and 15 wt % biochar displayed comparatively lower relative resistance values across the same flow rate range. These results demonstrate a measurable change in resistance with increasing flow rate for all sensor compositions.

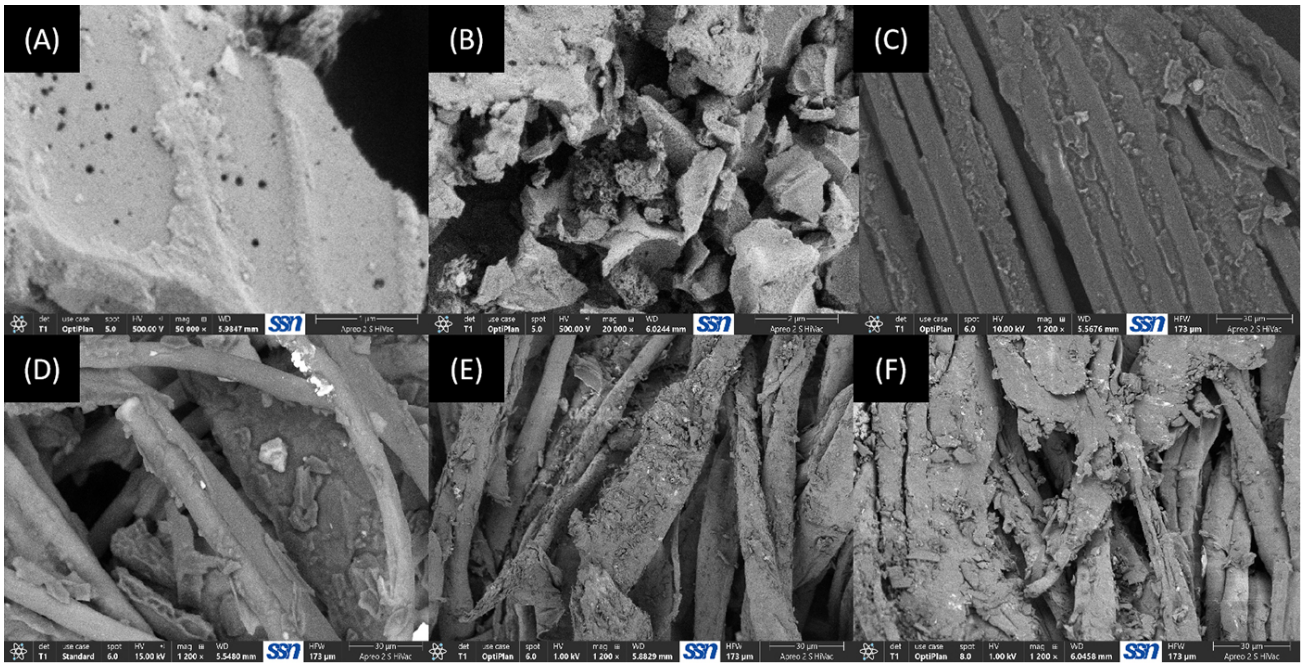

Fig. 7. Morphological SEM images of biochar and biochar-coated textile samples at different weight percentages. (A) Single Biochar, (B) Biochar, (C) 1 wt %, (D) 5 wt %, (E) 10 wt %, and (F) 15 wt % of biochar-coated samples. SEM, scanning electron microscopy; scale bar = 1 μm in (A); scale bar = 2 μm in (B); scale bar = 30 μm in (C–F).

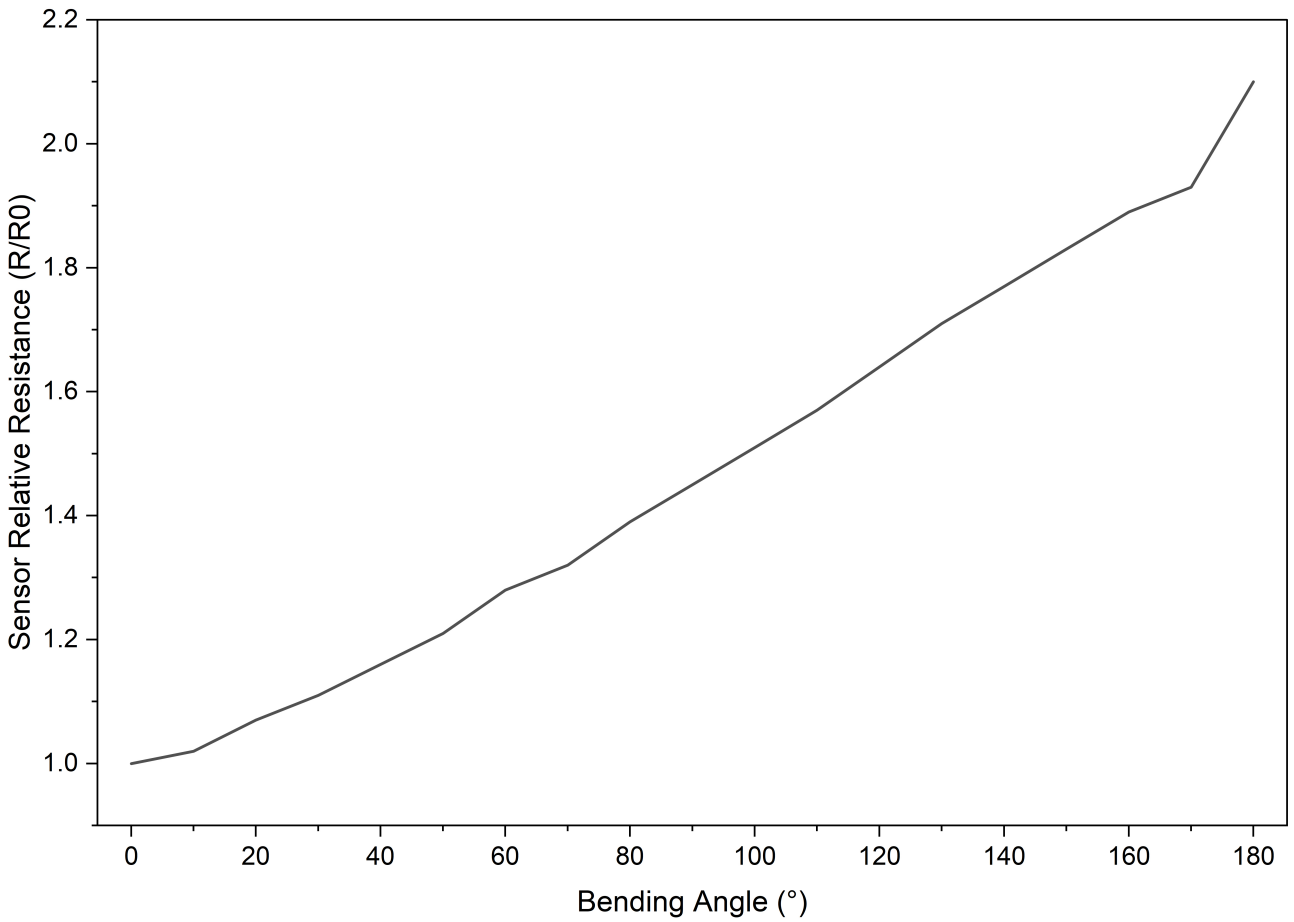

Fig. 8. Variation of the relative resistance (R/R_0) of the biochar-coated textile sensor under bending deformation.

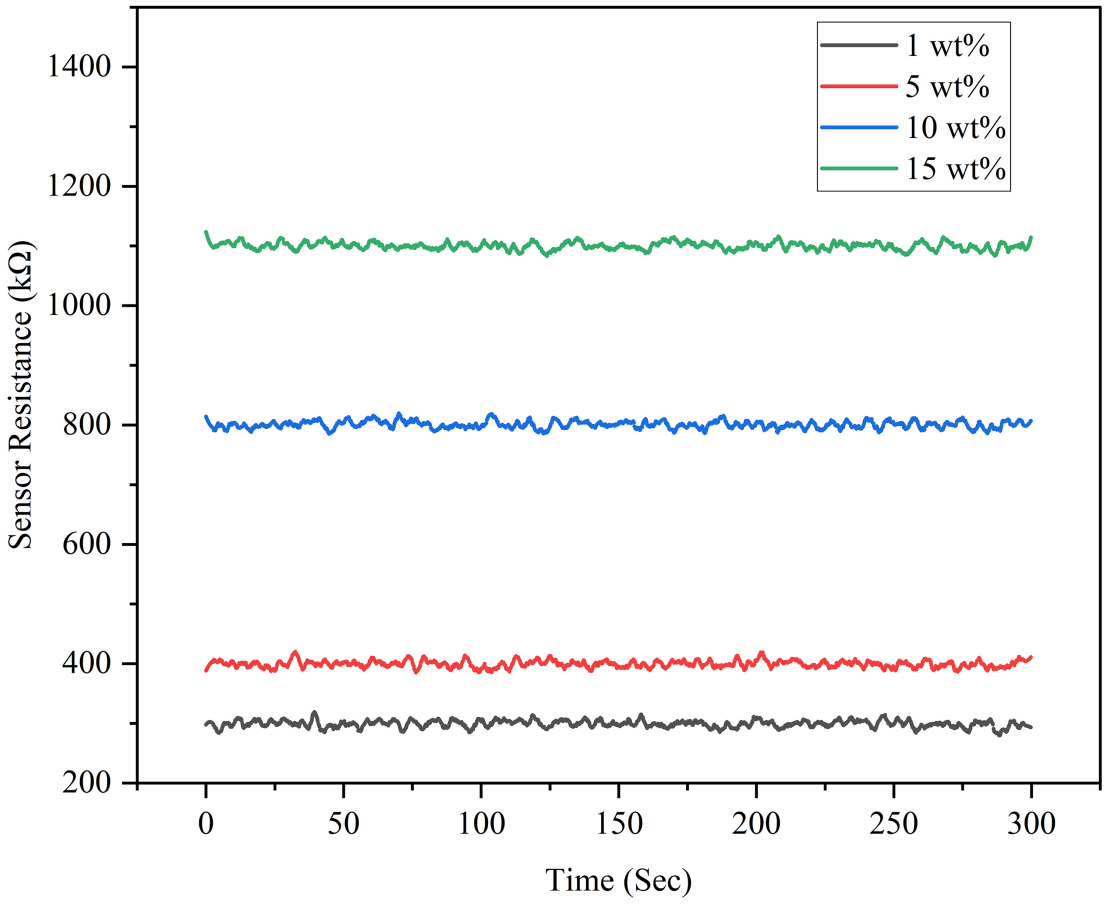

Fig. 9. Sensor resistances of biochar-based piezoresistive sensors *vs.* time variations.

Fig. 12A–D shows the variation in the sensor relative resistance (R/R_0) and water flow rate (Q) as a function of pump speed (rpm) for sensors containing 1 wt %, 5 wt %, 10 wt %, and 15 wt % biochar. As the pump speed increased, the water flow rate increased correspondingly for all compositions. The relative resistance responses of the sensors varied depending on the biochar loading in the coating layer. The 1 wt % sensor exhibited relatively higher resistance values with noticeable fluctuations, whereas the 5 wt % sensor exhibited a more stable resistance response across the tested pump speed range. The sensors containing 10 wt % and 15 wt % biochar displayed comparatively lower variations in relative resistance.

4. Discussion

4.1 Structural Characteristics of Biochar

The structural characteristics of the synthesized biochar were investigated using XRD and FTIR. The XRD pattern of the biochar, shown in Fig. 4, exhibits a broad diffraction peak centered at 2θ approximately 22–24°, corresponding to the (002) reflection of turbostratic carbon. The broad nature of this peak indicates that the carbon structure is predominantly disordered with limited long-range graphitic ordering. Such turbostratic carbon structures are commonly observed in biomass-derived carbon materials produced at moderate pyrolysis temperatures. Similar diffraction features have been reported for carbonized cellulose and other biomass-derived carbon materials used in flexible sensing applications [11,14,16].

The FTIR spectrum of the synthesized biochar, shown in Fig. 5, further confirms the presence of oxygen-containing functional groups on the biochar surface. The broad absorption band observed near 3350 cm^{-1} corresponds to O–H stretching vibrations, which are associated with hydroxyl groups originating from residual lignocellulosic components or adsorbed moisture [11,14]. The absorption band observed around 1625–1630 cm^{-1} corresponds to C=O stretching or aromatic C=C vibrations, indicating the formation of conjugated carbon domains during the pyrolysis process [11,15]. In addition, the band observed near 1175–1180 cm^{-1} corresponds to C–O stretching vibrations associated with alcohols, ethers, or phenolic functional groups [14,18]. The presence of these oxygen-containing functional groups suggests partial carbonization at the selected pyrolysis temperature and contributes to the surface polarity of the biochar particles, which may enhance the adhesion between the biochar coating and the textile fibers during the dip-coating process.

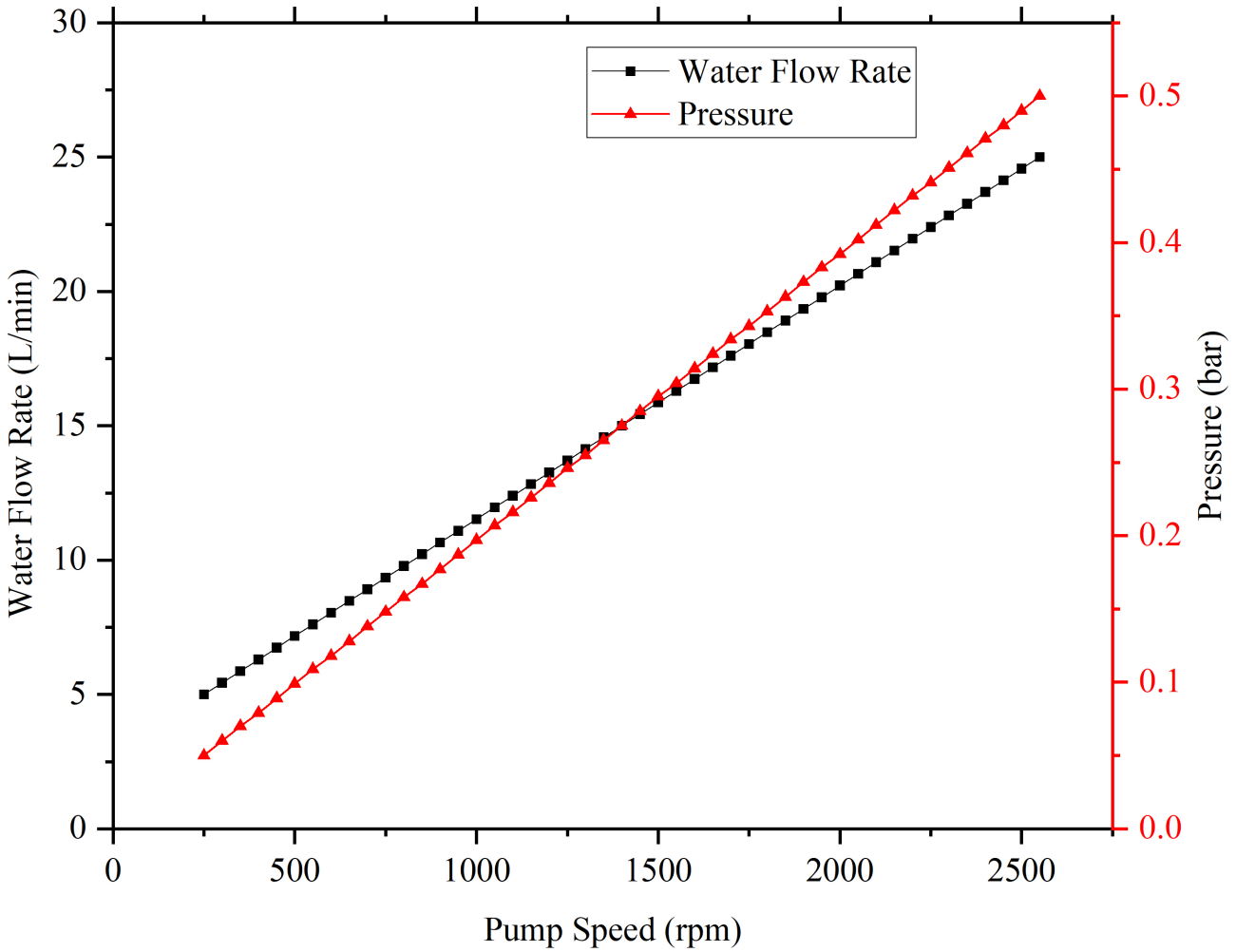

Fig. 10. Influence of pump speed variation on water flow rate and pressure.

The XRD patterns of the biochar-coated textile samples shown in Fig. 6 exhibit similar broad diffraction peaks centered at 2θ of approximately 22°, corresponding to the (002) reflection of turbostratic carbon. As the biochar concentration increases from 1 wt % to 15 wt %, the intensity of this peak gradually increases owing to the higher contribution of carbon domains deposited on the textile surface. However, the persistence of peak broadening across all compositions indicates that the deposited biochar maintains a predominantly amorphous or turbostratic carbon structure. This observation suggests that the coating process does not significantly alter the intrinsic structural characteristics of the biochar. Similar diffraction behavior has been reported for carbonized textile composites and biomass-derived carbon coatings used in flexible sensing materials [11,16].

4.2 Morphology and Particle Dispersion

The surface morphology of biochar-coated textile sensors plays a crucial role in determining the electrical conduction behavior and sensing performance of the device. The SEM images presented in Fig. 7A–F provide insight into the distribution of biochar particles on the textile fibers at different loading concentrations. The pristine biochar particles shown in Fig. 7A exhibit irregular shapes with distinct particle boundaries and porous surfaces, which are typical characteristics of biomass-derived carbon materials produced through pyrolysis. The aggregated biochar structure observed in Fig. 7B reveals an interconnected porous morphology with rough surface features, indicating the presence of a high surface area and inherent microporosity within the biochar particles. When deposited on the textile substrate through the dip-coating process, the morphology of the coating layer varies significantly with biochar concentration. At lower loading (1 wt %), the SEM image shown in Fig. 7C reveals that the biochar particles are sparsely distributed along the textile fibers, forming a thin and discontinuous coating layer. In this configuration, the underlying textile structure remains clearly visible, indicating limited surface coverage by the biochar particles. As the biochar concentration increases to 5 wt %, the SEM image shown in Fig. 7D reveals a more uniform particle distri-

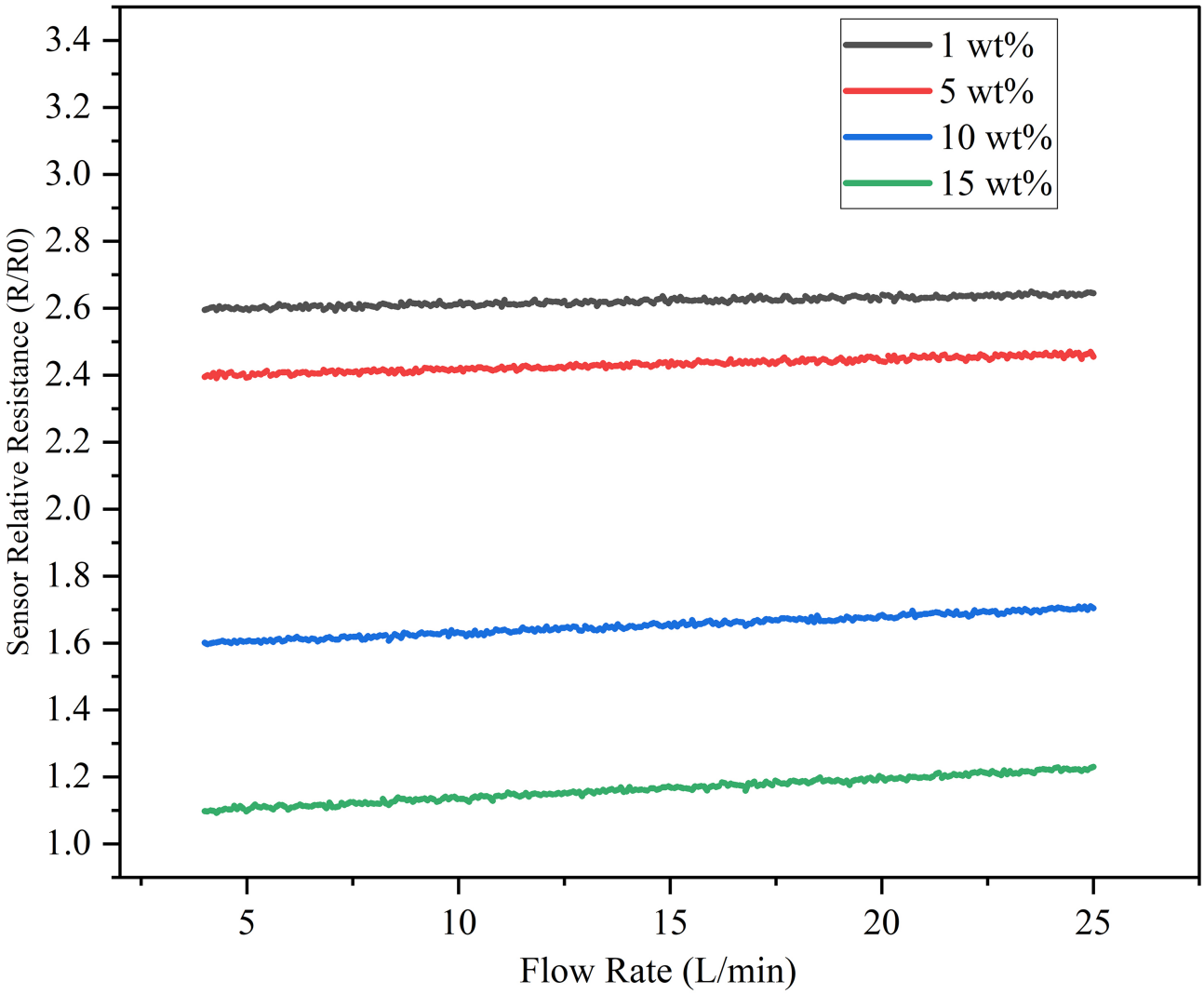

Fig. 11. Variation of the relative resistance (R/R_0) for all sensors with the flow rate.

bution along the textile fibers. The particles appear more evenly dispersed and form a relatively continuous coating layer across the fiber surface. Such particle distributions improve particle-particle contact and promote the formation of interconnected conductive pathways across the coating layer. However, further increasing the biochar concentration to 10 wt % and 15 wt % results in noticeable morphological changes. The SEM images presented in Fig. 7E and Fig. 7F reveal thicker coating layers and the presence of localized particle clusters on the fiber surfaces. These clusters indicate particle agglomeration caused by increased particle–particle interaction at higher filler concentrations. Such agglomeration can reduce dispersion uniformity and introduce irregular conductive pathways within the coating layer.

The observed morphological variations suggest that the particle distribution and coating thickness are strongly influenced by the biochar loading level. A relatively uniform particle distribution, as observed in the 5 wt % sample, facilitates better electrical connectivity between adjacent particles, whereas excessive particle clustering at higher concentrations may disrupt uniform conductive pathways. Similar morphological behavior has been reported in carbon-filled textile composites and flexible carbon-based sensing materials, wherein the filler concentration significantly influences conductive network formation and sensor performance [15,16].

4.3 Piezoresistive Sensing Mechanism

The sensing behavior of the biochar-coated textile sensor is governed by the piezoresistive effect, in which mechanical deformation leads to variations in the electrical resistance. In the present system, biochar particles deposited on the textile fibers form interconnected conductive pathways that enable electrical conduction through the coating layer. The electrical transport within this network is primarily controlled by the particle–particle contact resistance and electron tunneling between adjacent conductive domains. When water flows through the pipeline system, the resulting pressure induces slight mechanical deforma-

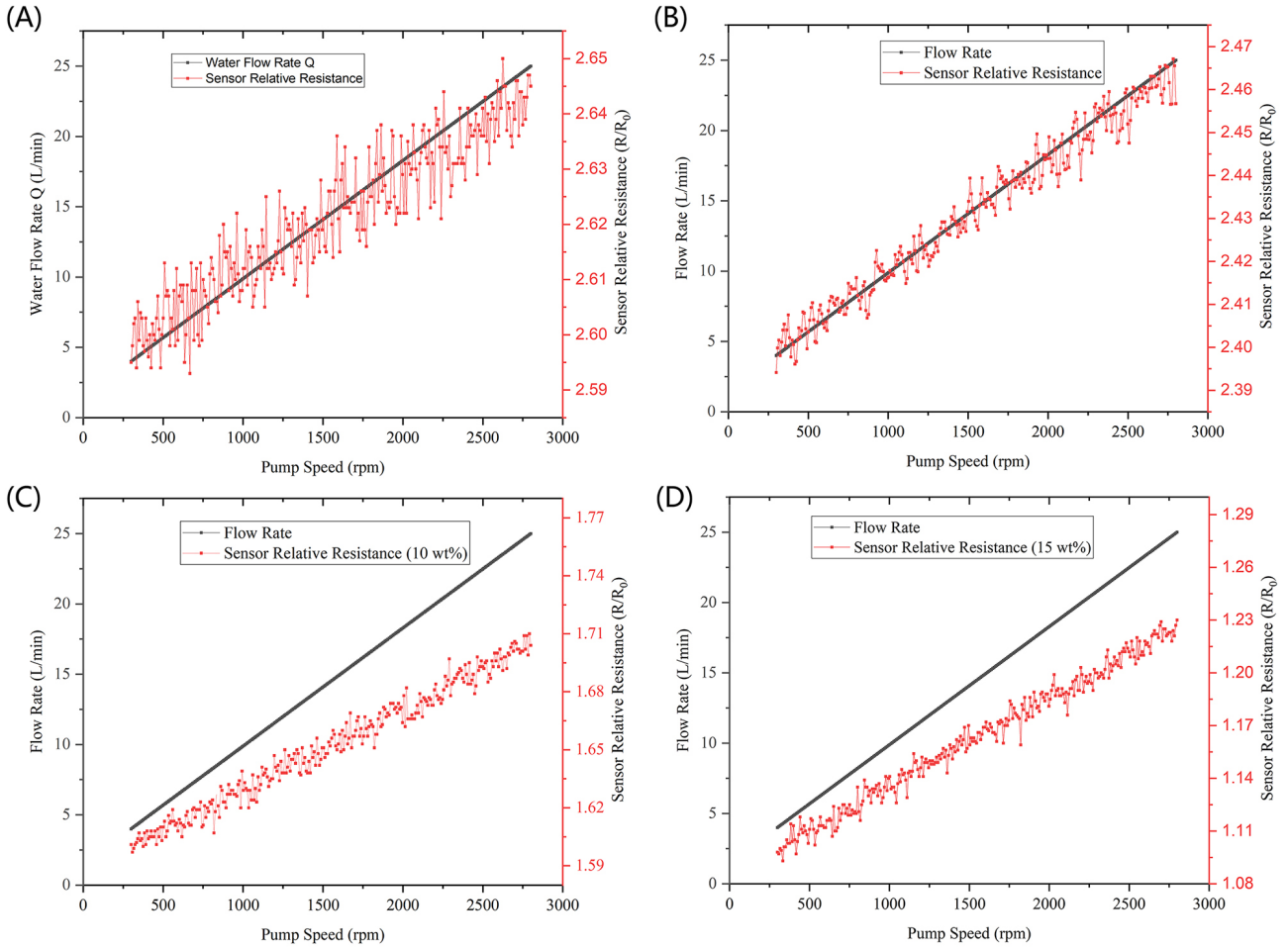

Fig. 12. Variation of flow rate and sensor relative resistance as a function of pump speed. (A) 1 wt %, (B) 5 wt %, (C) 10 wt %, (D) 15 wt %.

tion in the textile substrate. This deformation alters the distance and electrical contact between adjacent biochar particles within the coating layer, thereby modifying the conductive pathways across the sensor surface. As the water flow rate increases, the applied pressure increases correspondingly, producing measurable variations in the electrical resistance as observed in Fig. 11 and Fig. 12. In addition to flow-induced pressure, mechanical bending of the textile substrate also affects the electrical response of the sensor. During bending deformation, the textile fibers experience compression and stretching, which modify the electrical contact between conductive particles in the biochar coating. These structural changes lead to measurable resistance variations, confirming the piezoresistive nature of the sensing mechanism. In carbon-based flexible sensors, electrical conduction generally occurs through a combination of contact resistance modulation and electron tunneling effects between conductive particles. Mechanical deformation alters the distance between adjacent conductive domains, thereby influencing charge transport across the conductive network. Similar piezoresistive mechanisms have been widely reported in carbon nanotubes, graphene, and carbon-based textile sensors developed for flexible sensing applications [15,16].

4.4 Influence of Biochar Loading on Sensor Performance

The sensing performance of the biochar-coated textile sensors is strongly influenced by the biochar loading in the coating layer. Variations in the sensor response can be attributed to differences in particle dispersion, conductive network formation, and electrical connectivity between adjacent biochar particles. At a low loading (1 wt %), the SEM image in Fig. 7C shows that the biochar particles are sparsely distributed along the textile fibers, forming a thin and discontinuous coating layer. Such limited particle coverage restricts the formation of continuous conductive pathways, resulting in higher resistance values and greater fluctuations in the sensor response, as reflected in the resistance behavior shown in Fig. 11A. When the biochar loading is increased to 5 wt %, the particle distribution becomes more uniform along the textile fibers, as shown in Fig. 7D. This relatively continuous coating improves particle–particle contact and promotes the formation of interconnected conductive pathways across the coating sur-

Table 1. Comparison of the proposed biochar-coated textile sensor with previously reported flexible carbon-based sensors.

Sensor material	Key feature	Application	Reference
Carbonized cellulose fabric sensor	High flexibility and strain sensitivity	Wearable pressure sensing	[16]
Carbon aerogel-based sensor	Highly compressible porous carbon structure	Flexible pressure sensing	[14]
Biomass-derived carbon composite sensor	Sustainable carbon material with stable sensing behavior	Environmental sensing	[18]
Biochar-coated textile sensor	Sustainable biochar coating with stable R/R_0 response	Flow and pressure monitoring	This work

face. The improved conductive network enhances the stability of the electrical response and enables consistent resistance modulation under flow-induced pressure, as demonstrated in Fig. 11 and Fig. 12B.

However, further increasing the biochar concentration to 10 wt % and 15 wt % leads to thicker coatings and particle clustering, as observed in Fig. 7E and Fig. 7F. Such particle agglomeration reduces dispersion uniformity and introduces irregular conductive pathways, which can limit effective resistance modulation. This behavior is reflected in the comparatively lower resistance variation observed for higher-loading sensors in Fig. 11 and Fig. 12C,D. Similar effects of filler agglomeration on sensing performance have been reported in carbon-based flexible sensors [15,16]. Overall, the sensor containing 5 wt % biochar provides a favorable balance between conductive network formation, particle dispersion, and coating uniformity, resulting in a stable electrical response during flow sensing.

To place the performance of the developed biochar-coated textile sensor in context with that of previously reported flexible carbon-based sensors, a comparison with representative materials reported in the literature is summarized in Table 1 (Ref. [14,16,18]). The proposed biochar-coated textile sensor demonstrated stable resistance variation under flow-induced pressure while utilizing a sustainable biomass-derived carbon material and a dip-coating fabrication process.

4.5 Limitations

Although the developed biochar-coated textile sensor demonstrated promising performance for flow-induced pressure sensing, the present study focused on laboratory-scale validation under controlled experimental conditions. Long-term cyclic durability and environmental stability under repeated mechanical deformation have not been extensively investigated. In addition, the sensor performance was evaluated using a single pipeline setup, and further validation under different fluid conditions and practical operating environments is required. Future studies will focus on extended durability testing and the integration of the sensor into real-time monitoring systems for practical industrial applications.

5. Conclusions

This study demonstrates the suitability of biochar derived from *Senna siamea* biomass as a sustainable and effective material for improving the performance of piezoresistive-based sensors. Comprehensive structural, chemical, and morphological characterizations confirmed that the synthesized biochar exhibits favorable features, including inherent porosity and electrical conductivity, which are essential for reliable sensor operation and functional stability. Among the fabricated sensors with varying biochar concentrations, the 5 wt % biochar-coated sample demonstrated a favorable balance of sensitivity, stability, and linear response to changing flow rates and pressure. However, excessive biochar loading resulted in morphological agglomeration and diminished electrical response, underscoring the need for optimized loading. The dip-coated sensors responded reliably in both static and dynamic environments, reinforcing their applicability in real-time flow and pressure monitoring in biomedical and industrial contexts. Overall, this work highlights the effectiveness of incorporating biochar into textile substrates to develop cost-efficient and high-performance sensing devices, offering a promising route toward scalable and environmentally sustainable sensor technologies.

Abbreviations

SEM, scanning electron microscopy; FESEM, field-emission scanning electron microscope; FTIR, Fourier transform infrared spectroscopy; XRD, X-ray diffraction.

Availability of Data and Materials

The datasets generated and analyzed during the current study are available from the corresponding author upon reasonable request.

Author Contributions

BSRR conducted the experiments, performed data analysis, and prepared the original manuscript draft. VSR contributed to the conceptualization and design of the study, supervised the research, provided resources and facilities, and reviewed and revised the manuscript for important intellectual content. Both authors read and approved the final manuscript and agree to be accountable for all aspects of the work.

Ethics Approval and Consent to Participate

Senna siamea biomass was used in this study for biochar production. The plant material was collected from naturally available sources in Tamil Nadu, India. The collection and use of the plant material complied with relevant institutional, national, and international guidelines and regulations. No protected, endangered, or regulated plant species were involved in this study.

Acknowledgment

The authors sincerely acknowledge the support and facilities provided by the Department of Mechanical Engineering, Sri Sivasubramaniya Nadar College of Engineering, for conducting this research.

Funding

This research received no external funding.

Conflicts of Interest

The authors declare no conflicts of interest.

Declaration of AI and AI-Assisted Technologies in the Writing Process

The manuscript has been prepared by the authors based on original research work. Grammarly was used only to improve clarity, grammar, and readability of the text. No AI tools were used to generate scientific content, experimental data, analysis, or conclusions presented in this study. The authors confirm that all scientific interpretations and results are original and developed independently. After using this tool, the authors reviewed and edited the content as needed and take full responsibility for the content of the publication.

References

[1] Wang M, Wang G, Zheng M, Liu L, Xu C, Liu Z, et al. High-performance flexible piezoresistive pressure sensor based on multi-layer interlocking microstructures. Journal of Materials Chemistry A. 2024; 12: 22931–22944. https://doi.org/10.1039/D4TA03758H

[2] Kim M, Doh I, Oh E, Cho Y. Flexible Piezoelectric Pressure Sensors Fabricated from Nanocomposites with Enhanced Dispersion and Vapor Permeability for Precision Pulse Wave Monitoring. ACS Applied Nano Materials. 2023; 6: 22025–22035. https://doi.org/10.1021/acsanm.3c04030

[3] Zhuang Y, Li R, Jiao M, He X, Gu X, Huang S. A flexible piezoresistive pressure sensor based on a perovskite $MAPbBr_3$ nanocrystal-embedded polymer composite. Journal of Materials Chemistry C. 2024; 12: 10494–10503. https://doi.org/10.1039/D4TC01439A

[4] Krishnan A, Das S, Bhattacharjee M. Flexible Piezoresistive Pressure and Temperature Sensor Module for Continuous Monitoring of Cardiac Health. IEEE Journal on Flexible Electronics. 2023; 2: 350–357. https://doi.org/10.1109/JFLEX.2023.3243877

[5] Choi SB, Noh T, Jung SB, Kim JW. Stretchable Piezoresistive Pressure Sensor Array with Sophisticated Sensitivity, Strain-Insensitivity, and Reproducibility. Advanced Science (Weinheim, Baden-Wurttemberg, Germany). 2024; 11: e2405374. https://doi.org/10.1002/advs.202405374

[6] Han S, Li S, Fu X, Han S, Chen H, Zhang L, et al. Research Progress of Flexible Piezoresistive Sensors Based on Polymer Porous Materials. ACS Sensors. 2024; 9: 3848–3863. https://doi.org/10.1021/acssensors.4c00836

[7] Geng B, Zeng H, Luo H, Wu X. Construction of Wearable Touch Sensors by Mimicking the Properties of Materials and Structures in Nature. Biomimetics (Basel, Switzerland). 2023; 8: 372. https://doi.org/10.3390/biomimetics8040372

[8] Chen J, Xia X, Yan X, Wang W, Yang X, Pang J, et al. Machine Learning-Enhanced Biomass Pressure Sensor with Embedded Wrinkle Structures Created by Surface Buckling. ACS Applied Materials & Interfaces. 2023; 15: 46440–46448. https://doi.org/10.1021/acsami.3c06809

[9] Xu K, Tang Y, Liang J, Zhao T, Guo H. Flexible capacitive pressure sensor sensitized by tilted micropillar structures fabricated by two-photon polymerization. Journal of Materials Science: Materials in Electronics. 2024; 35: 1579. https://doi.org/10.1007/s10854-024-13350-5

[10] Sengupta D, Kottapalli AGP. Nanomaterials-Based Bioinspired next Generation Wearable Sensors: a State-of-the-Art Review. Advanced Electronic Materials. 2024; 10: 2300436. https://doi.org/10.1002/aelm.202300436

[11] Yang M, Wang Z, Jia Q, Xiong J, Wang H. Bio-Skin-Inspired Flexible Pressure Sensor Based on Carbonized Cotton Fabric for Human Activity Monitoring. Sensors (Basel, Switzerland). 2024; 24: 4321. https://doi.org/10.3390/s24134321

[12] Zhao Y, Liu L, Li Z, Wang F, Chen X, Liu J, et al. Facile fabrication of highly sensitive and durable cotton fabric-based pressure sensors for motion and pulse monitoring. Journal of Materials Chemistry C. 2021; 9: 12605–12614. https://doi.org/10.1039/D1TC02251B

[13] Yang W, Han X, Yin C, Zhang X, Peng Q, Yi C. Biomass carbon nanosphere-based flexible pressure sensors for motion capture and health monitoring. Composites Communications. 2024; 51: 102041. https://doi.org/10.1016/j.coco.2024.102041

[14] Wei L, Wu Z, Tang S, Qin X, Xiong Y, Li J, et al. Tracheid-inspired nanoarchitectured carbon-based aerogels with ultra-compressibility for wearable piezoresistive sensors. Carbon. 2023; 203: 386–396. https://doi.org/10.1016/j.carbon.2022.11.081

[15] Yang W, Qin Y, Wang Z, Yu T, Ge Z. Recent Advances in the Development of Flexible Sensors: Mechanisms, Materials, Performance Optimization, and Applications. Journal of Electronic Materials. 2022; 51: 6735–6769. https://doi.org/10.1007/s11664-022-09922-y

[16] Choi H, Sun J, Ren B, Cha S, Lee J, Lee B, et al. 3D textile structure-induced local strain for highly amplified piezoresistive performance of carbonized cellulose fabric-based pressure sensors for healthcare monitoring. Chemical Engineering Journal. 2022; 450: 138193. https://doi.org/10.1016/j.cej.2022.138193

[17] Amjadi M, Kyung KU, Park I, Sitti M. Stretchable, Skin-Mountable, and Wearable Strain Sensors and Their Potential Applications: A Review. Advanced Functional Materials. 2016; 26: 1678–1698. https://doi.org/10.1002/adfm.201504755

[18] Rahman SA, Khan SA, Iqbal S, Khadka IB, Rehman MM, Jang J, et al. Hierarchical Porous Biowaste-Based Dual Humidity/Pressure Sensor for Robotic Tactile Sensing, Sustainable Health, and Environmental Monitoring. Advanced Energy and Sustainability Research. 2024; 5: 2400144. https://doi.org/10.1002/aesr.202400144

[19] Trung TQ, Lee NE. Flexible and Stretchable Physical Sensor Integrated Platforms for Wearable Human-Activity Monitoringand Personal Healthcare. Advanced Materials (Deerfield

Beach, Fla.). 2016; 28: 4338–4372. https://doi.org/10.1002/adma.201504244
[20] Geng D, Chen S, Chen R, You Y, Xiao C, Bai C, et al. Tunable Wide Range and High Sensitivity Flexible Pressure Sensors with Ordered Multilevel Microstructures. Advanced Materials Technologies. 2022; 7: 2101031. https://doi.org/10.1002/admt.202101031
[21] Someya T, Bao Z, Malliaras GG. The rise of plastic bioelectronics. Nature. 2016; 540: 379–385. https://doi.org/10.1038/nature21004
[22] Li Y, Lei X, Guo D, Zhao Y, Zeng Z, Yi L, et al. Laser-Induced Skin-like Flexible Pressure Sensor for Artificial Intelligence Speech Recognition. ACS Applied Materials & Interfaces. 2024; 16: 10380–10388. https://doi.org/10.1021/acsami.3c15844
[23] Xu S, Xu Z, Li D, Cui T, Li X, Yang Y, et al. Recent Advances in Flexible Piezoresistive Arrays: Materials, Design, and Applications. Polymers. 2023; 15: 2699. https://doi.org/10.3390/polym15122699
[24] Chen Y, Lv C, Ye X, Ping J, Ying Y, Lan L. Hydrogel-based pressure sensors for electronic skin systems. Matter. 2025; 8: 101992. https://doi.org/10.1016/j.matt.2025.101992
[25] Peng Y, Yang N, Xu Q, Dai Y, Wang Z. Recent Advances in Flexible Tactile Sensors for Intelligent Systems. Sensors (Basel, Switzerland). 2021; 21: 5392. https://doi.org/10.3390/s21165392
[26] David AG, Samsingh Ramalingam V, Florence Sundarsingh E. Integrating neural network in advanced flow sensors for enhanced fluid flow characterization in conduit using carbon black. Proceedings of the Institution of Mechanical Engineers, Part C: Journal of Mechanical Engineering Science. 2025; 239: 2415–2423. https://doi.org/10.1177/09544062241305303